# / Review

# Dual Engineering of Olivetolic Acid Cyclase and Tetraketide Synthase for the Formation of Longer Alkyl-Chain Olivetolic Acid Analogs and Their Antibacterial Activities

Hiroyuki Morita

*Institute of Natural Medicine, University of Toyama, 2630 Sugitani, Toyama 930–0194, Japan.*

Received October 9, 2023

**Among presently used pharmaceuticals, about 60% were developed from natural products with unique chemical diversity and biological activities. Hence, the discovery of new bioactive compounds from natural products is still important for further drug development. In addition, breakthroughs in synthetic biology have also begun to produce many useful compounds through manipulations of the biosynthetic genes for secondary metabolites. Theoretically, this approach can also be exploited to generate new unnatural compounds by intermixing the genes from different biosynthetic pathways and/or engineering the secondary metabolite enzyme(s) with expanded substrate and product specificities. $\Delta^9$-Tetrahydrocannabinol ($\Delta^9$-THC), the heat-decarboxylated tetrahydrocannabinolic acid ($\Delta^9$-THCA) produced by *Cannabis sativa*, is the most important therapeutic cannabinoid due to its useful pharmacological features, such as analgesic, anti-emetic, anti-inflammatory, and anti-epileptic activities. In the structures of cannabinoids, the resorcinyl alkyl chain is a critical pharmacophore, and the therapeutic effects of $\Delta^9$-THC can be enhanced by converting the pentyl ($C_5$) moiety at C-3 to other acyl moieties. Thus, the expansion of unnatural cannabinoids with different C-3 alkyl moiety analogs might establish an excellent platform for the further development of therapeutically beneficial cannabinoids. This article reviews the structure-based dual engineering of both enzymes responsible for the formation of the resorcinyl core of $\Delta^9$-THC and describes the effect of C-6 alkyl-length extension of olivetolic acid, along with related analogs, on the antibacterial activities against *Bacillus subtilis* and *Staphylococcus aureus*.**

**Key words** enzyme engineering, crystal structure analysis, cannabinoid, antibacterial activity

## 1. Introduction

$\Delta^9$-Tetrahydrocannabinol ($\Delta^9$-THC) and cannabidiol (CBD) are pharmacologically interesting phytocannabinoids produced by *Cannabis sativa*, and are derived from tetrahydrocannabinolic acid ($\Delta^9$-THCA) and cannabidiolic acid (CBDA) *via* heat-decarboxylation[1–6] (Figs. 1, 2). The pharmacological activities of these cannabinoids principally occur through their interactions with two G-protein-coupled receptors (GPCRs), cannabinoid receptors (CB1 and CB2), which mediate the biological effects of the human endocannabinoid system for the treatment of chronic pain, stress, anxiety, depression, and insomnia.[2,7–10] $\Delta^9$-THC and CBD are also active at molecular targets outside the endocannabinoid system, in which several therapeutic targets, multiple signaling pathways, and ion channels are intricately involved.[3] Due to their unique pharmacological activities, cannabis strains containing $\Delta^9$-THCA and CBDA have been approved as medicines for the treatment of chronic pain in adults. Recently, cannabis has also been reported to improve the symptoms associated with diseases such as pain, spasticity, nausea, multiple sclerosis, epilepsy, and glaucoma, thus raising expectations for the use of cannabis as a new medicine.[11–14] However, because of the acute effects of $\Delta^9$-THC and CBD, such as psychoactive effects causing minor changes in psychomotor and cognitive functions, mild euphoria, a "high" state, and a relaxed state, their use requires great caution, which has highly restricted their medicinal applications. Therefore, attention has recently turned to other non-psychoactive cannabinoids such as cannabigerol (**1b**), cannabigerolic acid (**2b**), CBDA, and cannabichromene (CBC) (Fig. 1).

Among these non-psychoactive cannabinoids, CBG, the heat-decarboxylated product of CBGA, biosynthesized *via* the formation of olivetolic acid (**3b**) from *n*-hexanoyl-CoA (**5b**) and three malonyl-CoAs in *Cannabis sativa*, has recently received keen attention as a promising drug candidate (Figs. 1, 2). Structurally, **1b** consists of an alkylresorcinol core with a

This review of the author's work was written by the author upon receiving the 2023 Pharmaceutical Society of Japan Award for Divisional Scientific Promotion.

e-mail: hmorita@inm.u-toyama.ac.jp

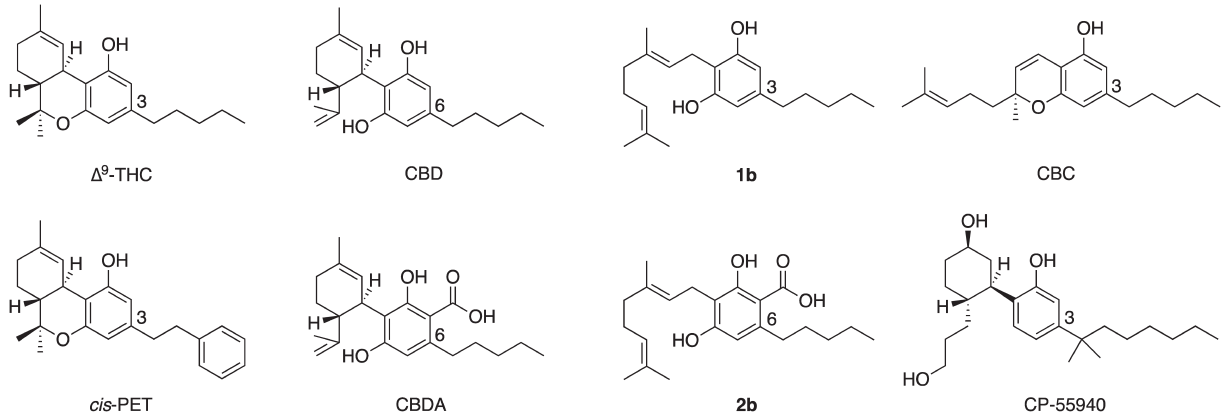


Fig. 1. Structures of $\Delta^9$-THC and Related Cannabinoids

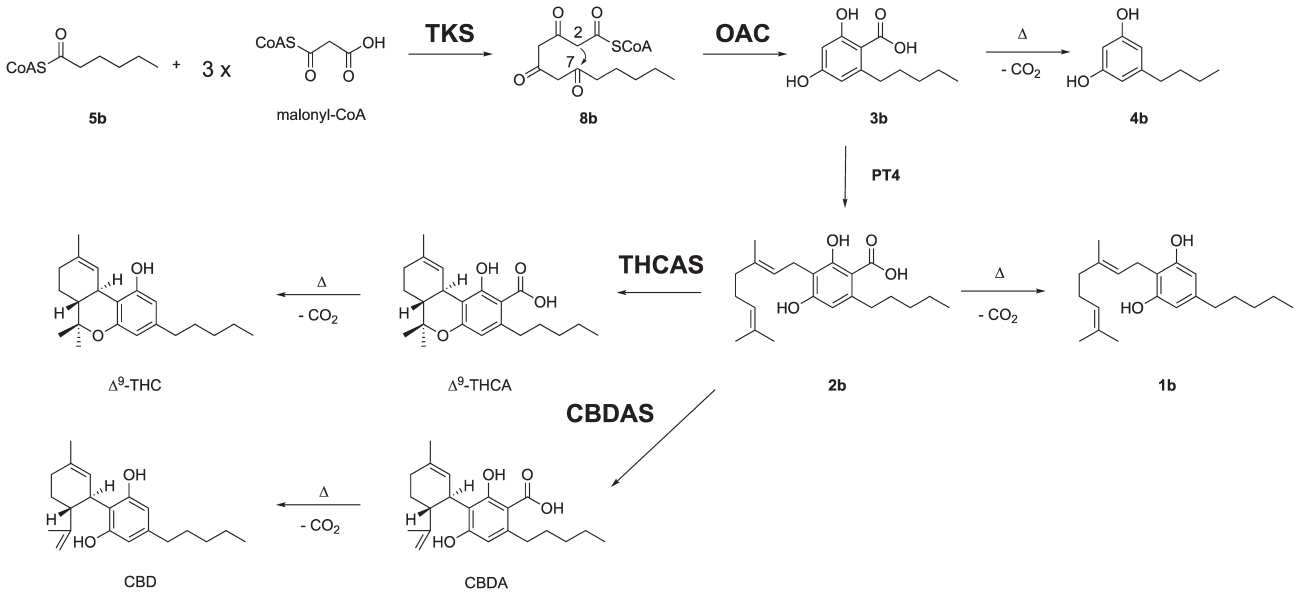


Fig. 2. Biosynthesis of $\Delta^9$-THCA and CBDA and the Decarboxylative Productions of **1b**, **4b**, $\Delta^9$-THC, and CBD

geranyl moiety at C-5. It lacks the psychoactive side effects of $\Delta^9$-THC, and acts as a potent $\alpha$2-adrenoceptor agonist and a moderate 5-hydroxytryptamine type 1A ($5\text{-HT}_{1A}$) receptor competitive antagonist[15,16] (Fig. 1). In addition, **1b** and **2b** reportedly exhibit good antibacterial activities against drug-resistant *Staphylococcus aureus*.[17] More recent studies reported that **2b** and CBDA have remarkable antiviral activities against severe acute respiratory syndrome coronavirus-2 (SARS-CoV-2) and its emerging variants, B.1.1.7 and B.1.351.[18] Although they have different side chains (monoterpenyl for **2b** and cyclohexene terpene ring for CBDA), equal effectiveness against SARS-CoV-2 and emerging mutants has been reported for both compounds, indicating that the olivetol core might be a crucial pharmacophore for acting on the SARS-CoV-2 spike protein. Compound **3b**, the initial common biosynthetic intermediate of cannabinoids (Fig. 2), also exhibits moderate

***Biography***

*Hiroyuki Morita obtained his Ph.D. in 2001 from University of Shizuoka under the direction of Professor Hiroshi Noguchi. After a year of postdoctoral research with Professor John C. Vederas at the University of Alberta in Canada (2001–2002), he returned to Japan to investigate the structural enzymology of protein kinases and plant polyketide synthases as a Postdoctoral Fellow at Mitsubishi Chemical Corporation (2002–2004) and Mitsubishi Kagaku Institute of Life Sciences (2004–2008). In 2008, he returned to the University of Shizuoka as an Assistant Professor (2008–2009), and then moved to the Laboratory of Natural Chemistry at the Graduate School of Pharmaceutical Sciences, The University of Tokyo as an Assistant Professor (2009–2012). He is now a Professor at the Institute of Natural Medicine, University of Toyama (2012–). His current research is focused on the engineering of secondary metabolite enzymes to generate new bioactive compounds.*

Hiroyuki Morita

anticonvulsant activity comparable to CBD, a known anticonvulsant cannabinoid, in a mouse model of Dravet syndrome, despite its low brain penetration.[19]

Meanwhile, the discovery of CBD and $\Delta^9$-THC analogs with an *n*-heptyl moiety, from the Italian FM2 cannabis variety, demonstrated that these new cannabinoids possess significant binding affinity against the human CB1 receptor, with equal potency to the full CB1 agonist CP55940[20] (Fig. 1), suggesting the potential of *n*-pentyl side chain modifications as biological activity modulators. In addition, investigations of (−)-*cis*-perrottetinene (*cis*-PET), the C-3 phenylethyl derivative of $\Delta^9$-THC produced by the liverwort *Radula* genus (Fig. 1), showed that this analog penetrates the brain and induces effects such catalepsy, hypothermia, and analgesia in a CB1 receptor-dependent manner, with fewer $\Delta^9$-THC-related side effects.[21] Furthermore, the elongation of the C-3 side chain of $\Delta^9$-THC reportedly increased its affinity for the cannabinoid receptors, suggesting that the C-3 alkyl side chain is one of the most critical pharmacophores in cannabinoids such as $\Delta^9$-THC. Therefore, the creation of $\Delta^9$-THC and **1b** and **2b** analogs with other alkyl-chains is expected to facilitate the development of better cannabinoid medicines. However, the complicated structure with two stereocenters has prevented the efficient chemical production of $\Delta^9$-THC and its and related analogs.[22]

As a different approach, a yeast expression system producing $\Delta^9$-THCA was recently developed by incorporating four biosynthetic genes, tetraketide synthase (TKS), olivetolic acid cyclase (OAC), geranylpyrophosphate : olivetolate geranyltransferase (PT4), and tetrahydrocannabinolic acid synthase (THCAS), into *Saccharomyces cerevisiae*[23] (Fig. 2). Thus, by exploiting this system with some modifications, $\Delta^9$-THCA, **1b**, and **2b** analogs are expected to be efficiently produced. Indeed, $\Delta^9$-THCA analogs with butyl, hexyl, 3-methylpentyl, 1-pentenyl and 1-hexynyl groups at C-6 have been successfully generated by supplying the corresponding fatty acids in the culture medium of the yeast expression system[23] (Fig. 3). However, this system cannot be used to generate $\Delta^9$-THCA analogs with alkyl side chains longer than an *n*-heptyl moiety, as verified from the absence of the corresponding **3b** analogs in the products. The inability of the system to produce $\Delta^9$-THCA analogs with longer alkyl side chains might be due to issues with the ability of TKS and/or OAC to accept longer alkyl substrates, such as *n*-decanoyl-CoA (**5d**) by TKS and a linear *n*-nonyltetra-*β*-ketide-CoA (**8d**) by OAC. Accordingly, engineered TKS and/or OAC will be required to generate $\Delta^9$-THCA and **1b** and **2b** analogs with longer alkyl moieties by the yeast expression system.

This paper reviews recent advancements in the engineering of TKS and OAC, obtained during the course of our research. The structure-guided engineering studies successfully expanded the substrate specificities of both enzymes up to a dodecanoyl ($C_{12}$) substrate to generate 2,4-dihydroxy-6-undecylbenzoic acid (**3e**). The antibacterial activities of **3b** and its analogs, as well as their derivatives, against *S. aureus* and *Bacillus subtilis* will also be discussed.

## 2. Crystal Structure Analysis of OAC

OAC is the only known plant polyketide cyclase that catalyzes the C7/C2 aldol cyclization of a linear *n*-pentyltetra-*β*-ketide-CoA (**8b**) produced by TKS, to generate **3b**[24] (Fig. 2). To the best of our knowledge, the substrate specificity of OAC for CoA thioesters with acyl moieties longer than the pentyl moiety has never been reported. However, TKS belongs to a type III polyketide synthase (PKS) family.[25] These well-studied enzymes have broad substrate specificity and produce diverse product analogs by condensing various acyl-CoAs as the starter substrate with malonyl-CoA as the extender substrate.[26–29] Although TKS reportedly accepts butyryl (**5a**)-, isovaleryl-, and octanoyl (**5c**)-CoAs as the starter substrate for condensation with two malonyl-CoAs, to produce the corresponding triketide-*α*-pyrones,[24] the production of longer alkyltetra-*β*-ketide-CoAs, such as *n*-heptyltetra-*β*-ketide-CoA (**8c**) from **5c** and three malonyl-CoAs, has never been reported. Given the previous findings on type III PKSs, it is not surprising that CoA thioesters with acyl moieties longer than a heptyl moiety could also be used as substrates. Based on this hypothesis, we decided to start this study from the engineering of OAC. However, the most beneficial three-dimensional information, such as sterically important neighboring amino acids, had not been reported.

We solved the crystal structure of OAC complexed with **3b** at 1.70 Å resolution (PDB code: 5B09)[30,31] (Figs. 4, 5). OAC adopts a dimeric $\alpha+\beta$ barrel (DABB) fold by forming an asymmetric dimer, and compound **3b** was accommodated within the interior of the $\alpha+\beta$ barrel of each monomer. The OAC crystal structure thus suggested that the OAC active sites might be located in the $\alpha+\beta$ barrel of each monomer. Further detailed analysis of the active site unveiled the presence of a 9 Å-long hydrophobic pocket; namely, the pentyl-binding pocket, in the active site cavity. The pentyl moiety of **3b** was accommodated in this pocket. Furthermore, the His78 side

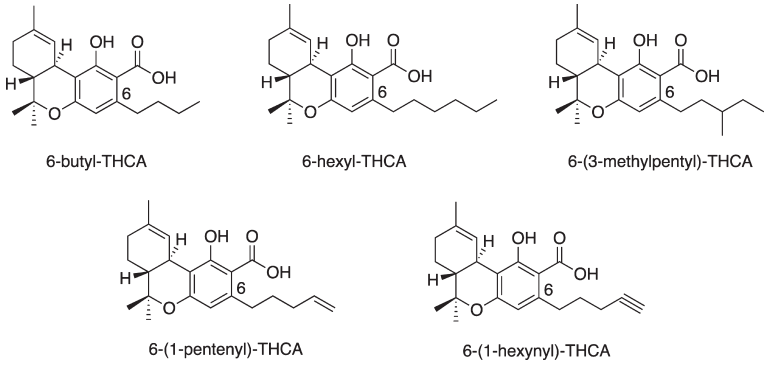


Fig. 3. $\Delta^9$-THC Analogs with Butyl-, Hexyl-, 3-Methylpentyl-, 1-Pentenyl-, and 1-Hexynyl Moieties Produced by the Yeast Expression System

chain protruded toward C-1 and C-6 of **3b**, which respectively correspond to C-2 and C-7 of the aldol cyclization points on the substrate **8b** in the active site. The His78 side chain also formed a hydrogen bonding network with the Tyr72 side chain. Taken together, these observations strongly suggested that the pentyl-binding pocket found in the OAC active site cavity accommodates the pentyl moiety of the substrate, while His78 and Tyr72 function as the catalytic residues of OAC.

These findings are further supported by mutagenesis experiments, which revealed that the substitutions of Ile7, Phe24, Tyr27, and Val59, lining the pentyl-binding pocket, with bulkier amino acids decreased the **3b**-forming activity by 15–70%, compared with that of wild type OAC. Furthermore, the substitutions of His78 and Tyr72 with other amino acids completely abolished the **3b**-forming activity. The crystal structures of the OAC Y27W, I7F, and V59M mutants (PDB codes: 5B0D, 5B0B, and 5B0E, respectively) indicated that the only significant differences between these mutants and wild-type OAC were the reduced sizes of the pentyl-binding pockets, which eventually led to decreased activity. In contrast, the crystal structures of the OAC H78S and Y72F mutants (PDB codes: 5B0G and 5B0F) revealed that the only significant differences between these mutants and wild-type OAC were the disruptions of the hydrogen-bond network between His78 and Tyr72, which resulted in the loss of activity. These results implied that the pentyl-binding pocket of OAC plays a crucial role to secure the pentyl moiety of the substrate during the OAC catalytic reaction, while His78 and Tyr72 might act as acid/base catalysts to produce **3b**. However, the amino acid residues responsible for the cleavage of the thioester bond of the substrate or its product, as well as the aromatic cyclization after the C7/C2 aldol ring-closure reaction, could not be identified in the crystal structure of OAC. These results strongly suggested that OAC catalyzes the C7/C2 aldol cyclization by locking the pentyl moiety of the substrate within the hydrophobic pocket and subsequently abstracting a proton from C-2 of the substrate with His78 activated by Tyr72, to cyclize the polyketide portion of the substrate, and then releases the cyclized product. Finally, this cyclized product is presumably converted to **3b** through non-enzymatic aromatization and thioester cleavage (Fig. 6). Thus, the OAC crystal structure indicated that the pentyl-binding pocket is crucial for control-


Fig. 4. Primary Sequence Comparison of OAC with Other DABB Proteins

The catalytic residues of OAC and the equivalent residues of the functionally unidentified AtHS1 (48% amino acid sequence identity) and SP1 (38% amino acid sequence identity) proteins are highlighted in blue (numbering according to OAC:**3b**). PECPS shares 48 and 38% amino acid sequence identities with AAtHs1 and SP1, respectively. GenBank accession numbers are as follows: OAC (JN679224), *Arabidopsis thaliana* AtHS1 (Uniprot code Q9LUV2), *Populus tremula* SP1 (P0A881).

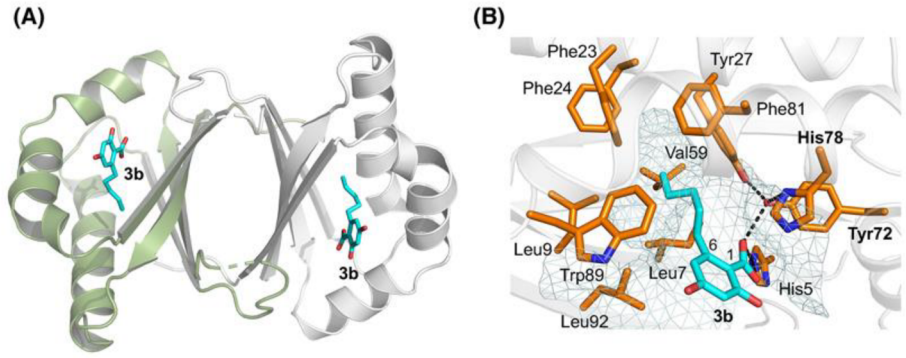


Fig. 5. Crystal Structure of OAC Complexed with **3b**

(**A**) Overall structure of OAC. (**B**) Close-up view of the active site cavity. The catalytic residues His78 andTyr72 are highlighted with bold fonts. The hydrogen bonds are indicated as dashed lines. The active site cavity is represented by a pale blue mesh surface model.

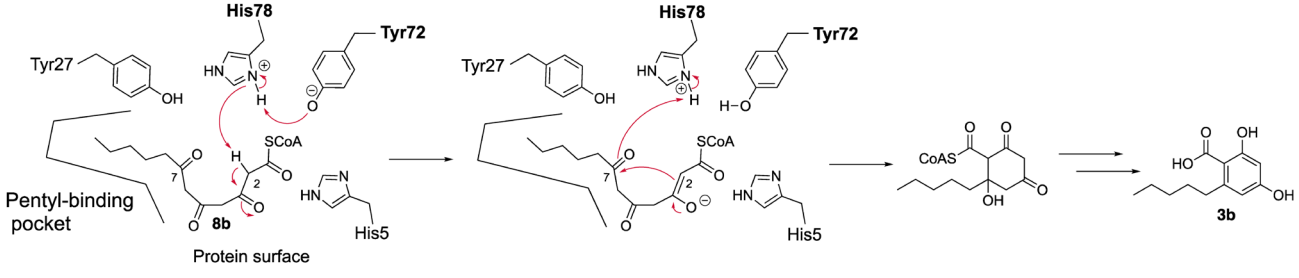


Fig. 6. Proposed Mechanism for **3b** Formation by OAC

ling the alkyl moiety preference of the substrate.

## 3. Effect of OAC Mutations on 3b Analog-Forming Activity

The aim of this study was to develop OAC mutant(s) capable of producing **3b** analogs with a bulkier alkyl moiety than the pentyl moiety. This could be achieved by expanding the size of the pentyl-binding pocket. Hence, by combining these features, we attempted to create a pentyl-binding pocket that can generate **3b** analogs with longer alkyl moieties by replacing the amino acid residues with similar or less bulky hydrophobic amino acid residues.[32)]

The pentyl-binding pocket is composed of nine amino acid residues: Ile7, Leu9, Phe23, Phe24, Tyr27, Val59, Phe81, Trp89, and Leu92 (Fig. 5). Among them, Tyr27, Phe24, and Val59 form the bottom region of the pentyl-binding pocket. Two residues, Phe24 and Val59, were replaced by Leu and Met, respectively, when the aforementioned crystal structure analysis of OAC was performed, and their roles in the catalytic reaction of OAC have already been demonstrated.[31)] However, in that case, the OAC mutant enzymes, in which these amino acids were replaced with Ala, formed inclusion bodies during heterologous expression in *Escherichia coli*, and soluble enzymes could not be obtained even by refolding methods. Therefore, we newly constructed the OAC F24I/V and OAC V59I/L single mutants. Although the OAC F24V mutant formed inclusion bodies in *E. coli*, the OAC F24I and V59I/L single mutants were obtained as soluble enzymes. Notably, Tyr27 is involved in the formation of not only the bottom, but also the side wall of the pentyl-binding pocket, and thus its substitution with a much less bulky amino acid may disrupt the overall structure of the enzyme. Thus, we decided to re-examine the **3**-forming activities of the OAC Y27F/L/M/W single mutants that were previously prepared for the crystal structure analysis of OAC. In addition, we performed co-incubation assays of TKS and OACs, in which *n*-hexanoyl-CoA (**5b**), *n*-octanoyl-CoA (**5c**), *n*-decanoyl-CoA (**5d**), *n*-lauroyl-CoA (**5e**), and *n*-myristoyl-CoA (**5f**) were added with malonyl CoA as substrates, since an alkyltetra-$\beta$-ketide-CoA as the OAC substrate is unstable and cannot be used directly in the *in vitro* enzyme reaction. The enzyme products detected by this study are summarized in Fig. 7,[32)] among which the olivetol (**4**), triketide-$\alpha$-pyrone (**6**), and tetraketide-$\alpha$-pyrone (**7**) types of compounds are known by-products produced by TKS and/or other type III PKSs.

First, the **3b**-forming activities of the OAC mutants were investigated. The LC-MS analysis revealed that all tested mutants retained their **3b**-forming activities (Fig. 8). However, their activities were decreased compared with that of the wild type, except for the OAC Y27F mutant, which showed a 62% increase in its **3b**-forming activity. The crystal structure of the OAC Y27F mutant (PDB code: 5B0C) indicated that the Y27F substitution disrupted the hydrogen bond between Tyr27 and Tyr72 observed in the wild-type OAC crystal structure, but maintained all the conformations of the active-site residues in the mutant enzyme, in locations and orientations very similar to those in the wild-type.[31)] Presumably, the effect of the loss of the hydroxy group of Tyr27 on the hydrogen bond network at the active site increased both the hydrophobicity of the pentyl-binding pocket and the electrostatic interaction between Tyr72 and His78, which further enhanced the **3b**-forming activity.

Next, the pholic acid (**3c**)-forming activity was evaluated. Interestingly, wild-type OAC produced **3c**, which has never been reported, and this activity was slightly increased when the OAC F24I mutant was co-incubated with TKS (Fig. 8). However, the production of 2,4-dihydroxy-6-heptylbenzoic acid (**3d**) was not observed in any OAC enzyme reactions, including the wild-type OAC. These observations suggested that further mutagenesis of OAC would be necessary to expand its function.

To obtain useful information for further mutagenesis, the

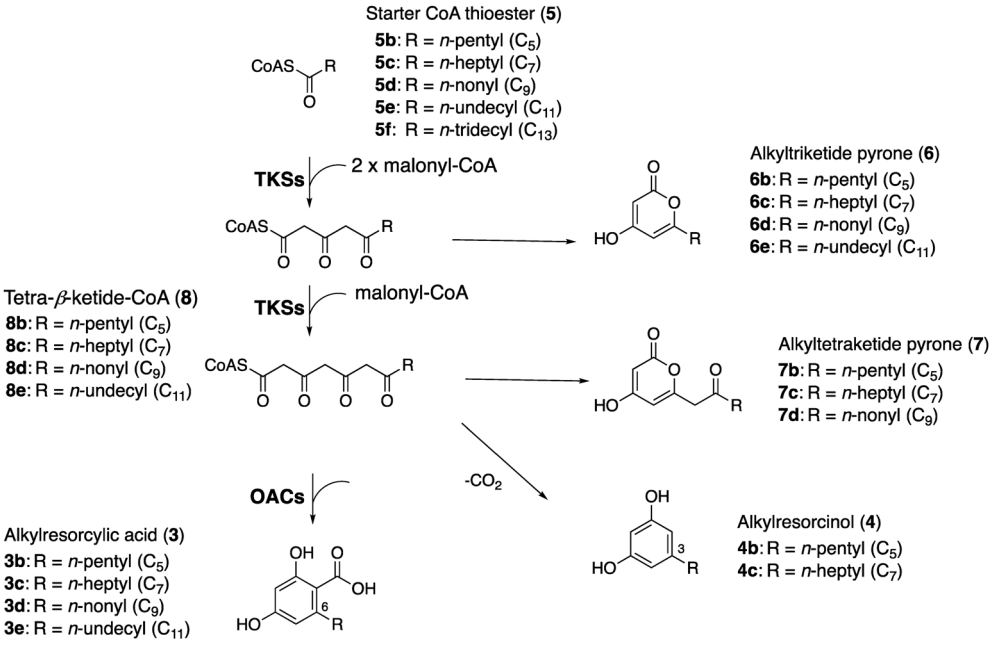


Fig. 7. Alkylresorcylic Acids, Alkylresorcinols, and Alkyltri- and Alkyltetraketide Pyrones Detected in the Reaction Mixtures of OACs and TKSs, Using Linear Fatty Acyl-CoAs and Malonyl-CoA as Starter Substrates

crystal structure of OAC F24I complexed with **3c** was solved at 1.38 Å resolution (PDB: 7W6E)[32] (Fig. 9). The structure revealed that the substitution of Phe27 with Ile extended the depth of the pentyl-binding pocket to 12 Å, and this elongated pocket could actually accommodate the heptyl moiety of **3c**. Furthermore, the structure also showed some remaining space between the tip of the heptyl moiety of **3c** and the bottom of the pentyl-binding pocket, suggesting the possibility that the OAC F24I mutant could bind **3b** analogs with longer alkyl moieties. Thus, the crystal structure of the OAC F24I mutant complexed with **3d** (PDB code: 7W6F) was solved, and the results clearly indicated that the F24I substitution creates a sufficiently large pentyl-binding hydrophobic pocket to accommodate **3d**. Based on the crystal structure analyses, the OAC F24I mutant likely accepts **8c** produced by TKS, to generate **3d**. Notably, this observation was not consistent with the actual enzyme reaction results described above, indicating that TKS, together with OAC, might also be a limiting factor for the formation of **3b** analogs with longer alkyl moieties. Thus, we shifted our focus to engineering studies of TKS.

## 4. Effects of TKS Mutations on 3b-Analog-Forming Activity

Kearsey *et al.* reported the crystal structure of TKS complexed with CoA-SH (PDB ID: 6GW3)[33] (Figs. 10, 11), which indicated that its active site is apparently smaller than those of most other type III PKSs. This might be the reason why TKS was unable to produce **8d** as the OAC substrate for the formation of **3d**, when *n*-decanoyl-CoA (**5d**) and malonyl-CoA were added to the reaction mixture. In previous studies, the sizes and shapes of the active site cavity reportedly determined the substrate and product specificities of most type III PKSs.[26,27,34–36] In addition, the substrate specificity and number of malonyl-CoA condensations can be increased by expanding the active site volume. Therefore, the creation of a functionally expanded TKS mutant that can accept CoA thioesters with longer alkyl moieties as substrates to produce the required OAC substrates might be possible, if the depth of the TKS active site cavity can be extended.

The TKS engineering was performed based on the example of *Aloe arborescens* octaketide synthase (OKS), a type III PKS that produces SEK4b and SEK4 from the condensations of eight malonyl-CoAs in the *in vitro* enzyme reaction, although its function in plants still remains unclear.[32,37] OKS also reportedly has the ability to catalyze the decarboxylative condensation of *n*-eicosanoyl-CoA with three malonyl-CoAs, for the formation of the corresponding **7**.[37] Previous engineering of OKS indicated that the substitution of the active site

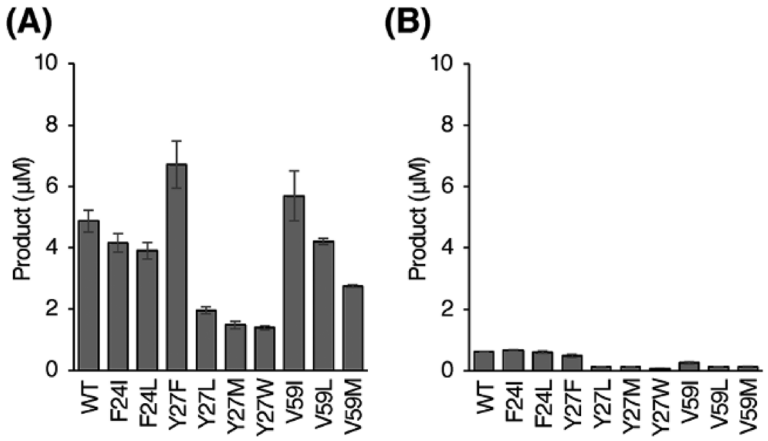


Fig. 8. Production of **3** by Combinations of OACs and Wild-Type TKS

(**A** and **B**) Production of (**A**) **3b** and (**B**) **3c** from the OAC and TKS coincubation assays. Data are presented as the mean ± S.D. (standard deviation, $n = 3$). WT: wild-type enzyme.

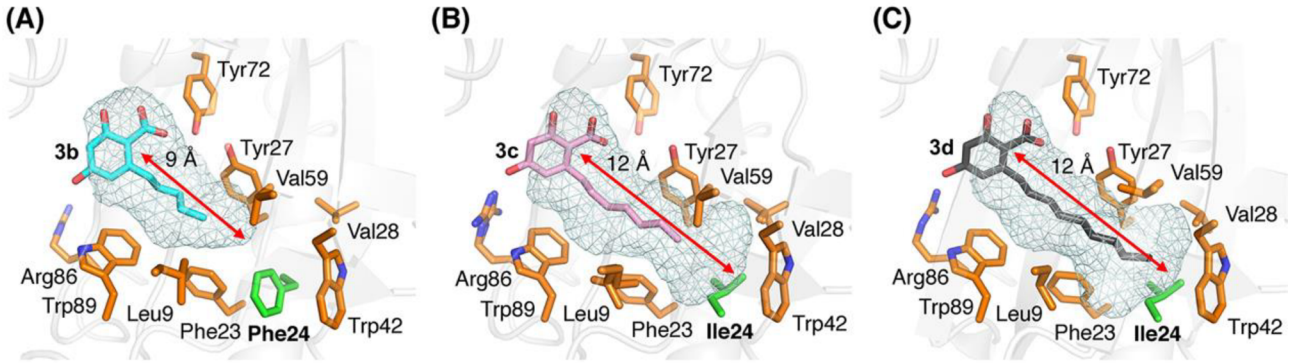


Fig. 9. Active Site Architectures of (**A**) Wild-Type OAC Complexed with **3b**, (**B**) OAC-F24I Mutant Complexed with **3c**, and (**C**) OAC-F24I Mutant Complexed with **3d**

The active site cavities are represented by pale blue mesh surface models. The Phe24 residue in the wild-type OAC is depicted by a black stick model and bold font. The Ile24 residues in the OAC F24I mutants are depicted by green stick models and bold fonts.

residue Gly207 with Met causes the loss of substrate specificity for fatty acyl-CoAs longer than **5e**.[37] The opposite case was found in the mutational studies of *A. arborescens* pentaketide chromone synthase (PCS), in which Met207, corresponding to Gly207 of OKS, was altered to Gly.[26] As a result, the five malonyl-CoA condensing- and pentaketide chromone-producing wild type PCS was converted to a SEK4b- and SEK4-producing enzyme like OKS. Our homology models of wild type OKS and its OKS G207M mutant enzymes, based on the crystal structure of the PCS M207G mutant, suggested that this was due to an active site cavity divided into two sections (Fig. 11). Interestingly, this newly observed pocket behind the active site cavity of the OKS G207M mutant is originally present in the crystal structure of TKS. Accordingly, Leu190 of TKS, corresponding to Gly207 of OKS, was substituted with Gly with the aim of expanding the active site cavity of the TKS L190G mutant, like the wild-type OKS. The crystal structure of the TKS L190G mutant complexed with **5e** at 2.10 Å resolution (PDB code: 7W6G) (Fig. 11) indicated that this L190G substitution successfully connected the active site cavity with the hidden pocket observed in wild type TKS to generate a longer active site cavity, with a length comparable to that of OKS.[37] Thus, we further investigated the abilities of wild-type OAC and its mutants with the use of this newly created TKS L190G mutant.

The co-incubation of the TKS L190G mutant and the wild type OAC or F24I mutant enzyme established that the **3b**-forming activities of both the wild-type OAC and its F24I mutant were slightly increased, compared with those in the assay with wild-type TKS[32] (Fig. 12). In this case, the **3b**-forming

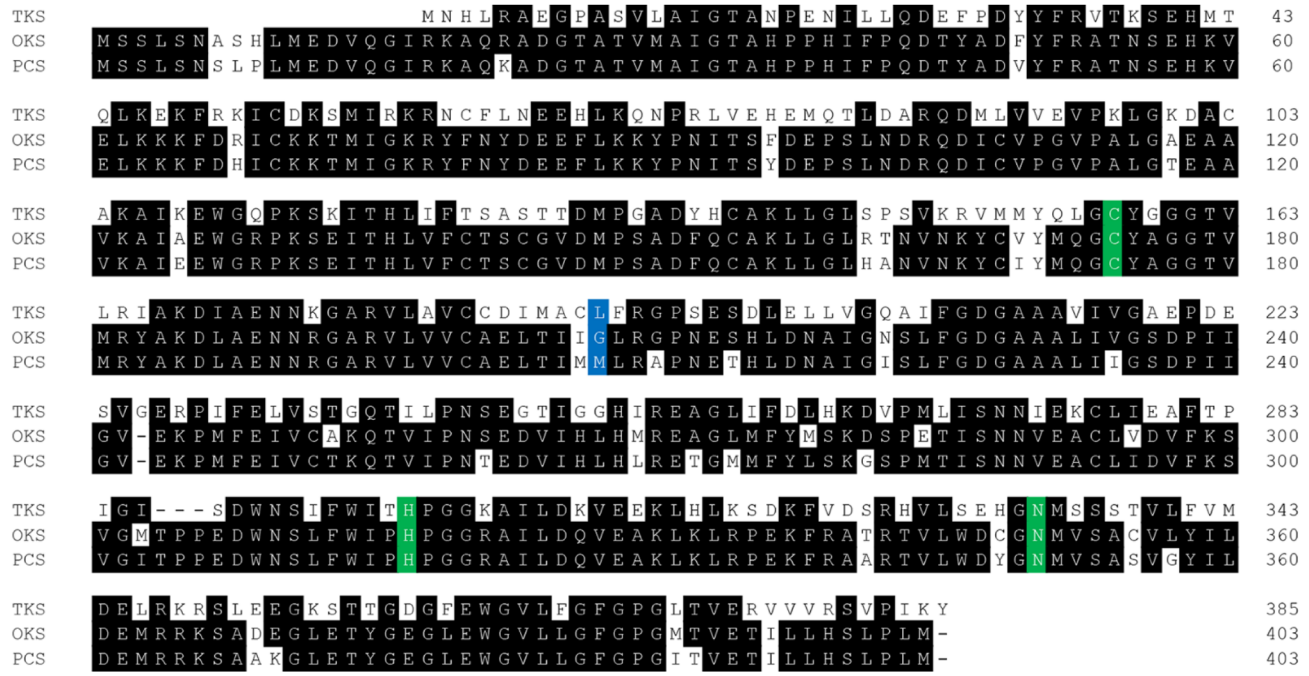


Fig. 10. Primary Sequence Comparison of TKS, OKS, and PCS

The catalytic residues of OAC and the equivalent residues are highlighted in green. TKS shares 53 and 52% amino acid sequence identities with OKS and PCS, respectively. GenBank accession numbers are as follows: TKS (AB164375), OKS (AY567707), PCS (AY823626).

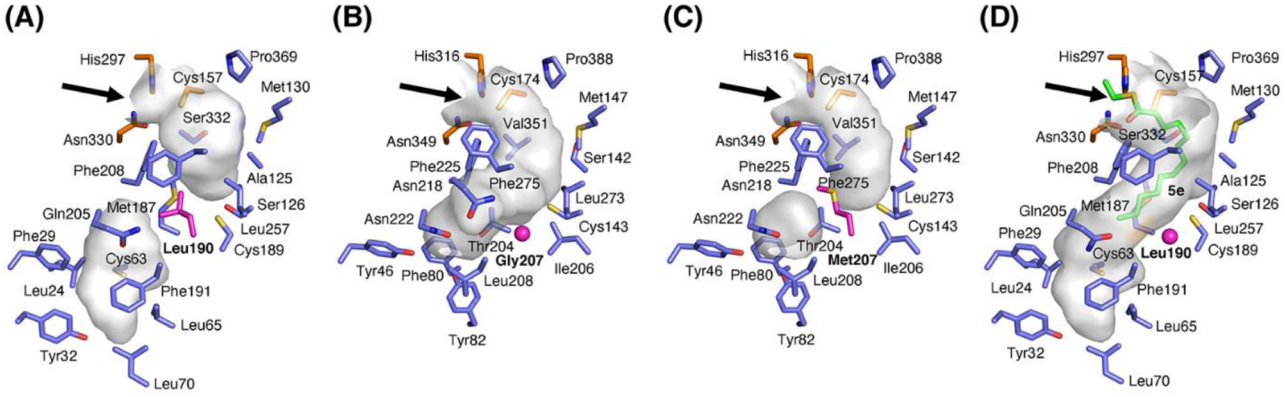


Fig. 11. Comparisons of the Active Site Architectures in (**A**) the Crystal Structure of TKS, (**B**) the Homology Models of (**B**) OKS and (**C**) the OKS G207M Mutant, and (**D**) the Crystal Structure of the TKS L190G Mutant

The catalytic triads involved in the substrate loading and decarboxylative malonyl-CoA condensations are shown as orange sticks. The homologous residues at Leu190 of TKS, Gly207 of OKS, Met207 of the OKS G207M mutant, and Gly190 of the TKS L190G mutant are depicted by pink stick models and bold fonts. The arrows indicate the active site entrances. A partial structure of **5b** bound in the crystal structure of the TKS L190G mutant is shown as a green stick model.

activity of wild-type OAC was higher than that of the OAC F24I mutant. However, the **3c**-forming activity of wild-type OAC was dramatically increased in combination with the TKS L190G mutant, relative to the wild-type TKS, and this activity was augmented with the OAC F24I mutant. The co-incubation assay using the TKS L190G mutant revealed that wild-type OAC naturally possessed weak **3d**-forming activity, which has never been reported, and this activity was further enhanced by about 10-fold in combination with the TKS L190G and OAC F24I mutants (Fig. 12). Finally, the co-incubation assay demonstrated that only the combination of the TKS L190G and OAC F24I mutants could generate 2,4-dihydroxy-6-undecylbenzoic acid (**3e**) (Fig. 12). Similar results were also observed with the combination of the TKS L190G and OAC F24L mutants, although the activities were weaker than those of OAC F24I mutant (Fig. 12). As a side note, the production of **3b** analogs with longer alkyl moieties than an undecyl moiety was not observed in other OAC mutants, even with the use of the TKS L90G mutant (Fig. 12). Taken together, the engineering of TKS and OAC successfully expanded the substrate specificities of both enzymes up to dodecanoyl substrates to generate **3e**, especially with the combined use of the TKS L190G and OAC F24I mutants.

In addition to the newly conferred **3b**- to **3e**-forming activities, the LC-MS analysis revealed that the pentaketide derivatives derived from the CoA thioesters **5b**, **5c**, **5d** and **5e** with four malonyl-CoAs were produced as the reaction products of OAC and/or its mutants in combination with the TKS L190G mutant. These pentaketide derivatives were deduced from their molecular weights, which correspond to the pentaketides.[32] Trace amounts of their production were also observed in the sole incubation of the TKS L190G mutant enzyme. The structures of these compounds have not been determined, due to their instability. However, considering their molecular weights, MS/MS fragments, and the catalytic properties of TKS and OAC, these compounds are proposed to be 3-(2′,4′-dihydroxyphenyl)-3-oxopropanoic acids with an alkyl moiety at the 6′-position (**9b**–**e**), which might be derived from a linear alkylpenta-*β*-ketide-CoA (**10b**–**e**) *via* the C4/C9 aldol cyclization reaction by OAC and/or its Phe24Ile/Leu mutant (Fig. 13). There are presently no reports on the specificity of OAC for the length of the substrate's polyketide portion. These observations suggested that OAC could be tolerant of the length of the polyketide portion.

## 5. Antibacterial Activities of 3b-Analogs and Its Related Compounds

As mentioned above, **1b** and **2b** have recently shown great promise as pharmaceutical seeds.[15–18] Compound **2b** is a C-3 geranylated compound of **3b**, and **1b** is a heat-decarboxylated product of **2b**. Compounds **1b** and **2b** could exhibit dramatically different biological activities than **3b** due to the presence of the geranyl moiety, which would enhance their hydrophobicity and improve their binding affinity to cells and fungi to exert their beneficial activities for humans, as previously reported for other prenylated compounds.[38,39] In this context, the **3b** analogs with longer alkyl moieties may also potentially be active compounds like **1b** and **2b**, due to their increased hydrophobicity from the longer C-6 alkyl moieties.[40]

In an attempt to identify their potential, the antibacterial activities of **3b**–**3e** against *S. aureus* were evaluated as a preliminary investigation.[40] To this end, the antibacterial activities of varinolic acid (**3a**) and 2,4-dihydroxy-6-tridecylbenzoic acid (**3f**), the **3b** analogs with butyl and tridecyl moieties at C-6, respectively (Fig. 14), were also assessed to further evaluate the chain-length effects. The antibacterial potentials of all

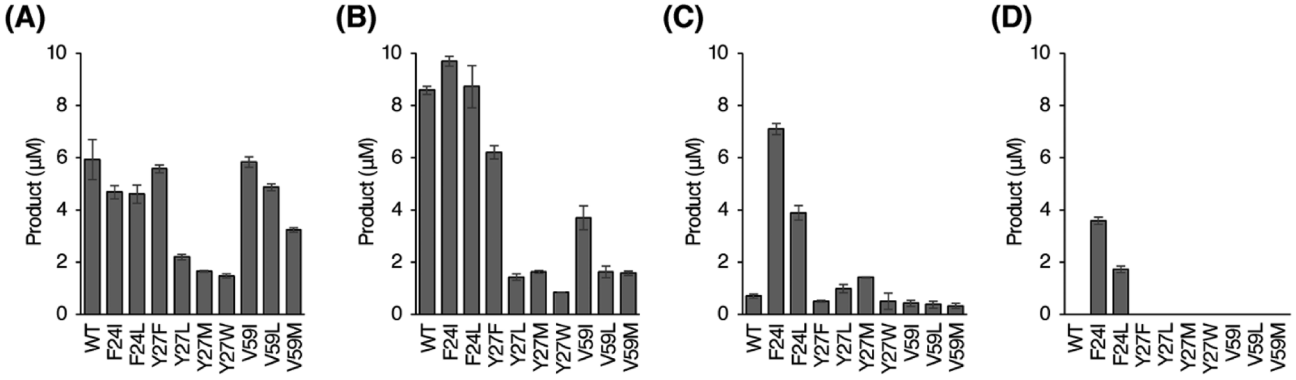


Fig. 12. Production of **3** by Combinations of OACs and the TKS L197G Mutant

(**A**–**D**) Production of (**A**) **3b**, (**B**) **3c**, (**C**) **3d**, and (**D**) **3e** from the coincubation assays of OACs and the TKS L197G mutant. Data are presented as the mean ± S.D. (standard deviation, $n = 3$). WT: wild type enzyme.

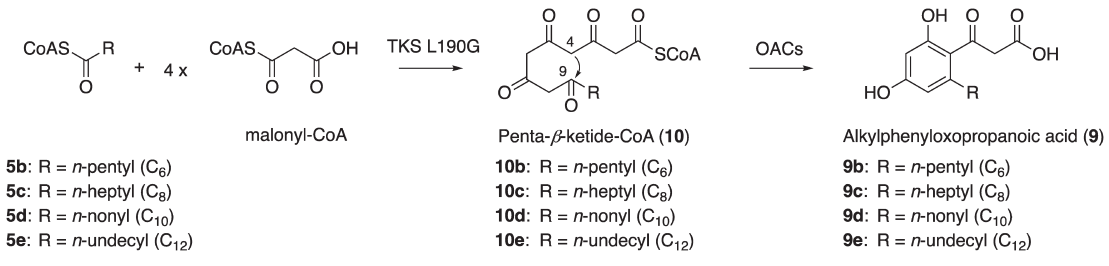


Fig. 13. Plausible Structures of **9b**–**e** and the Proposed Pathway for Their Formation by TKS L190G and Wild-Type OAC or Its OAC F24I Mutant

compounds were also tested against *B. subtilis* in this study, since **1b** reportedly showed antibacterial activity against this Gram-positive bacterium.[41] Since the use of *in vitro* reactions to obtain sufficient amounts of the compounds for the antibacterial assay is cumbersome, given the substrate costs and the lack of the enzymes to generate **3f**, all the **3b** analogs were chemically synthesized[40] according to the previously reported method.[42] The corresponding **2**-series (**2a**–**f**), **1**-series (**1a**–**f**), and **4**-series (**4a**–**f**), as summarized in Fig. 14, were also chemically synthesized, to evaluate the chain-lengths effects of the synthesized **3**-series on the antibacterial activities.[40] As a side note, the syntheses of the **2**-series were achieved by semi-syntheses, in which the NphB G286S/Y288N double mutant[43] was used for the regiospecific geranylation of the **4**-series as mother compounds.

The antibacterial activities of the tested compounds are summarized in Table 1. The assay revealed that **3a** and **3b** lacked antibacterial activities against *B. subtilis* and *S. aureus*, while **3c**–**f** newly acquired antibacterial activities against both bacteria. The antibacterial activity of the **3**-series increased in an alkyl-chain length-dependent manner. Remarkably, the antibacterial activities of **3e** and **3f** against *B. subtilis* were enhanced to levels comparable with that of **2b**. In addition, the activities of the **3**-series tended to be as strong or stronger than those of the **4**-series. This analysis indicated that **2c** has the most potential against *B. subtilis* among the tested compounds, while **1b** and **1c** were the strongest compounds against *S. aureus*. Unlike the case of the **3**-series, where the chain-length-dependent activity was observed, the approximate chain-lengths of the alkyl moieties were observed in the **1**- and **2**-series ($C_6$- and $C_8$-lengths for the **1**-series and $C_8$ length for the **2**-series). An excessive increase of the hydrophobicity by the elongated alkyl moiety could have resulted in a lower intracellular concentration due to poor aqueous solubility, leading to the decreased antibacterial potentials observed in **2e** and **1d**. The modulation of the hydrophobic balance of the hydrophobic alkyl chains at C-3 and C-6 in **1b** and **2b** may be one of the key strategies to enhance the bioactivities of **2b** derivatives.

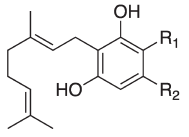


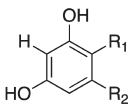


| | $R_1$ | $R_2$ | | $R_1$ | $R_2$ |
|---|---|---|---|---|---|
| **1a** | H | *n*-propyl ($C_3$) | **3a** | COOH | *n*-propyl ($C_3$) |
| **1b** | H | *n*-pentyl ($C_5$) | **3b** | COOH | *n*-pentyl ($C_5$) |
| **1c** | H | *n*-heptyl ($C_7$) | **3c** | COOH | *n*-heptyl ($C_7$) |
| **1d** | H | *n*-nonyl ($C_9$) | **3d** | COOH | *n*-nonyl ($C_9$) |
| **1e** | H | *n*-undecyl ($C_{11}$) | **3e** | COOH | *n*-undecyl ($C_{11}$) |
| **1f** | H | *n*-tridecyl ($C_{13}$) | **3f** | COOH | *n*-tridecyl ($C_{13}$) |
| **2a** | COOH | *n*-propyl ($C_3$) | **4a** | H | *n*-propyl ($C_3$) |
| **2b** | COOH | *n*-pentyl ($C_5$) | **4b** | H | *n*-pentyl ($C_5$) |
| **2c** | COOH | *n*-heptyl ($C_7$) | **4c** | H | *n*-heptyl ($C_7$) |
| **2d** | COOH | *n*-nonyl ($C_9$) | **4d** | H | *n*-nonyl ($C_9$) |
| **2e** | COOH | *n*-undecyl ($C_{11}$) | **4e** | H | *n*-undecyl ($C_{11}$) |
| **2f** | COOH | *n*-tridecyl ($C_{13}$) | **4f** | H | *n*-tridecyl ($C_{13}$) |

Fig. 14. Structures of Compounds **1a**–**f**, **2a**–**f**, **3a**–**f**, and **4a**–**f** Tested for the Antibacterial Activities

## 6. Conclusion

This review has discussed our recent advances in engineering studies of TKS and OAC, as well as the chain-length effects of the **1**–**4**-series. The introduction of these engineered biosynthetic enzymes into the $\Delta^9$-THCA-producing yeast expression system might expand the repertoire of cannabinoids with pharmaceutical potential, which could be further developed into useful medicines. In addition, the use of a biological system to produce cannabinoid analogs might provide a solution to the complex problem of obtaining various cannabinoids with unique side chains by chemical synthesis. The antibacterial results in this study also proved that, despite being intermediates in cannabinoid biosynthesis and even with simple structures, the addition of long alkyl moieties to **3b** indeed conferred some biological activity to the compounds. It will be particularly interesting to further evaluate these compounds with various alkyl-chain lengths for their neuron-related therapeutic potential, since the final cannabinoid products exert various biological actions in the central nervous system. The results obtained in this study have also provided insight into the biological activities of the **3**-series and the related analogs of the **1**-, **2**-, and **4**-series at the molecular level, which might ultimately lead to the development of pharmaceutical products. Considering the pharmacological activities of *cis*-PET, the C-3 phenylethyl derivative of $\Delta^9$-THC with fewer

Table 1. Antibacterial Activities of **1a**–**f**, **2a**–**f**, **3a**–**f**, and **4a**–**f**

| Compounds | MIC ($\mu$M) | |
|---|---|---|
| | *S. aureus* | *B. subtilis* |
| **1a** | 25 | 25 |
| **1b** | 2.5 | 3.13 |
| **1c** | 2.5 | 6.25 |
| **1d** | 6.25 | >200 |
| **1e** | 25 | >200 |
| **1f** | >200 | >200 |
| **2a** | 12.5 | 12.5 |
| **2b** | 3.13 | 2.5 |
| **2c** | 3.13 | 1.25 |
| **2d** | 12.5 | 3.13 |
| **2e** | 25 | 6.25 |
| **2f** | >200 | 50 |
| **3a** | >200 | >200 |
| **3b** | >200 | >200 |
| **3c** | 100 | 200 |
| **3d** | 12.5 | 25 |
| **3e** | 6.25 | 2.5 |
| **3f** | 6.25 | 2.5 |
| **4a** | >200 | >200 |
| **4b** | >200 | >200 |
| **4c** | 100 | 100 |
| **4d** | 12.5 | 12.5 |
| **4e** | 6.25 | 3.125 |
| **4f** | 200 | 12.5 |
| Ampicillin[a] | 0.15 | 0.15 |

*a*) Positive control. MIC: minimum inhibitory concentration.

psychological side effects, the creation of similar **3b** derivatives may also be fruitful. However, we have not succeeded in producing **3b** analogs with aromatic rings at C-6. This is due to the lack of a type III PKS capable of forming a linear aromatic tetra-$\beta$-ketide-CoA as the OAC substrate. We hope that such analogs can be enzymatically generated in the near future, with the discovery of type III PKSs that can generate aromatic products.

**Acknowledgments** These studies were performed at the Institute of Natural Medicine, University of Toyama. The author expresses sincere appreciation to Professor Ikuro Abe and Associate Professor Takahiro Mori of The University of Tokyo, and Emeritus Professor Hiroshi Noguchi of University of Shizuoka for fruitful discussions and encouragement. The author would like to thank past and present staff and students; Drs. Takashi Matsui, Takeshi Kodama, Yu Nakashima, Xinmei Yang, and Yuan-E Lee, and Ms. Xinrui Chen. This work has been supported in part by Grants-in-Aid for Scientific Research from the Ministry of Education, Culture, Sports, Science and Technology, Japan (JSPS KAKENHI Grants, 17H02203, JP19H04649, 22H02777).

**Conflict of Interest** The author declares no conflict of interest.

## References

1) de Meijer E. P. M., Bagatta M., Carboni A., Crucitti P., Moliterni V. M. C., Ranalli P., Mandolino G., *Genetics*, **163**, 335–346 (2003).
2) Russo E., Guy G. W., *Med. Hypotheses*, **66**, 234–246 (2006).
3) Turner S. E., Williams C. M., Iversen L., Whalley B. J., "Phytocannabinoids," Vol. 103, ed. by Kinghorn A. D., Falk H., Gibbons S., Kobayashi J., Springer, Switzerland, 2017, pp. 61–101.
4) Russo E. B., *Ther. Clin. Risk Manag.*, **4**, 245–259 (2008).
5) Baron E. P., *Headache*, **58**, 1139–1186 (2018).
6) Li H., Liu Y., Tian D., Tian L., Ju X., Qi L., Wang Y., Liang C., *Eur. J. Med. Chem.*, **192**, 112163 (2020).
7) Bow E. W., Rimoldi J. M., *Perspect. Medicin. Chem.*, **8**, PMC. S32171 (2016).
8) Wouters E., Walraed J., Banister S. D., Stove C. P., *Biochem. Pharmacol.*, **169**, 113623 (2019).
9) An D., Peigneur S., Hendrickx L. A., Tytgat J., *Int. J. Mol. Sci.*, **21**, 5064 (2020).
10) Mlost J., Bryk M., Starowicz K., *Int. J. Mol. Sci.*, **21**, 8870 (2020).
11) Hill K. P., Palastro M. D., Johnson B., Ditre J. W., *Cannabis Cannabinoid Res.*, **2**, 96–104 (2017).
12) Lakhan S. E., Rowland M., *BMC Neurol.*, **9**, 59 (2009).
13) Rocha F. C. M., Stéfano S. C., De Cássia Haiek R., Oliveira L. M. R., Da Silveira D. X., *Eur. J. Cancer Care* (Engl.), **17**, 431–443 (2008).
14) Stockings E., Zagic D., Campbell G., Weier M., Hall W. D., Nielsen S., Herkes G. K., Farrell M., Degenhardt L., *J. Neurol. Neurosurg. Psychiatry*, **89**, 741–753 (2018).
15) Pollastro F., Taglialatela-Scafati O., Allara M., Munoz E., Di Marzo V., De Petrocellis L., Appendino G., *J. Nat. Prod.*, **74**, 2019–2022 (2011).
16) Izzo A. A., Borrelli F., Capasso R., Di Marzo V., Mechoulam R., *Trends Pharmacol. Sci.*, **30**, 515–527 (2009).
17) Karas J. A., Wong L. J., Paulin O. K., Mazeh A. C., Hussein M. H., Li J., Velkov T., *Antibiotics*, **9**, 406 (2020).
18) van Breemen R. B., Muchiri R. N., Bates T. A., Weinstein J. B., Leier H. C., Farley S., Tafesse F. G., *J. Nat. Prod.*, **85**, 176–184 (2022).
19) Anderson L. L., Udoh M., Everett-Morgan D., Heblinski M., McGregor I. S., Banister S. D., Arnold J. C., *J. Cannabis Res.*, **4**, 1–9 (2022).
20) Citti C., Linciano P., Russo F., Luongo L., Iannotta M., Maione S., Laganà A., Capriotti A. L., Forni F., Vandelli M. A., Cannazza G., *Sci. Rep.*, **9**, 1–13 (2019).
21) Chicca A., Schafroth M. A., Reynoso-Moreno I., Erni R., Petrucci V., Carreira E. M., Gertsch J., *Sci. Adv.*, **4**, eaat2166 (2018).
22) Schafroth M. A., Mazzoccanti G., Reynoso-Moreno I., Erni R., Pollastro F., Caprioglio D., Botta B., Allegrone G., Grassi G., Chicca A., Gasparrini F., Gertsch J., Carreira E. M., Appendino G., *J. Nat. Prod.*, **84**, 2502–2510 (2021).
23) Luo X. Z., Reiter M. A., Keasling J. D., *Nature* (London), **567**, 123–126 (2019).
24) Gagne S. J., Stout J. M., Liu E., Boubakir Z., Clark S. M., Page J. E., *Proc. Natl. Acad. Sci. U.S.A.*, **109**, 12811–12816 (2012).
25) Taura F., Tanaka S., Taguchi C., Fukamizu T., Tanaka H., Shoyama Y., Morimoto S., *FEBS Lett.*, **583**, 2061–2066 (2009).
26) Abe I., Morita H., *Nat. Prod. Rep.*, **27**, 809–838 (2010).
27) Morita H., Abe I., Noguchi H., "Comprehensive Natural Products II: Chemistry and Biology," ed. by Liu H-W., Mander L., Elsevier, Oxford, U.K., 2010, pp. 171–225.
28) Morita H., Yamashita M., Shi S.-P., Wakimoto T., Kondo S., Kato R., Sugio S., Kohno T., Abe I., *Proc. Natl. Acad. Sci. U.S.A.*, **108**, 13504–13509 (2011).
29) Wang X., Gao B., Nakashima Y., Mori T., Zhang Z., Kodama T., Lee Y., Zhang Z., Wong C. P., Liu Q., Qi B., Wang J., Li J., Liu X., Abe I., Morita H., Tu P., Shi S.-P., *Nat. Commun.*, **13**, 348 (2022).
30) Yang X., Matsui T., Mori T., Taura F., Noguchi H., Abe I., Morita H., *Acta Crystallogr. F Struct. Biol. Commun.*, **71**, 1470–1474 (2015).
31) Yang X., Matsui T., Kodama T., Mori T., Zhou X., Taura F., Noguchi H., Abe I., Morita H., *FEBS J.*, **283**, 1088–1106 (2016).
32) Lee Y. E., Nakashima Y., Kodama T., Chen X., Morita H., *Org. Lett.*, **24**, 410–414 (2022).
33) Kearsey L. J., Prandi N., Karuppiah V., Yan C., Leys D., Toogood H., Takano E., Scrutton N. S., *FEBS J.*, **287**, 1511–1524 (2020).
34) Austin M. B., Noel J. P., *Nat. Prod. Rep.*, **20**, 79–110 (2003).
35) Morita H., Wong C. P., Abe I., *J. Biol. Chem.*, **294**, 15121–15136 (2019).
36) Morita H., Lee Y., Shi S.-P., *J. Nat. Med.*, **77**, 667–676 (2023).
37) Abe I., Oguro S., Utsumi Y., Sano Y., Noguchi H., *J. Am. Chem. Soc.*, **127**, 12709–12716 (2005).
38) Chen X., Mukwaya E., Wong M. S., Zhang Y., *Pharm. Biol.*, **52**, 655–660 (2014).
39) Kamanna K., Kamath A., "Modifications of biomolecules," ed. by Zhan X., Jabbari A., IntechOpen, London, 2022.
40) Lee Y. E., Kodama T., Morita H., *J. Nat. Med.*, **77**, 298–305 (2023).
41) Appendino G., Gibbons S., Giana A., Pagani A., Grassi G., Stavri M., Smith E., Rahman M. M., *J. Nat. Prod.*, **71**, 1427–1430 (2008).
42) Cochrane R. V., Sanichar R., Lambkin G. R., Reiz B., Xu W., Tang Y., Vederas J. C., *Angew. Chem.*, **128**, 674–678 (2016).
43) Valliere M. A., Korman T. P., Woodall N. B., Khitrov G. A., Taylor R. E., Baker D., Bowie J. U., *Nat. Commun.*, **10**, 565 (2019).